Corrosion resistance and antibacterial properties of copper coating deposited by cold gas spray

F. S. da Silva[a,b], N. Cinca[b], S. Dosta[b], I. G. Cano[b], J. M. Guilemany[b], C. S. A. Caires[c], A. R. Lima[c], C. M. Silva[c], S. L. Oliveira[c], A. R. L. Caires[c], A. V. Benedetti[a]*

[a] UNESP - São Paulo State University, Institute of Chemistry, Rua Prof. Francisco Degni, 55, P.O. Box 355, 14800-060, Araraquara, SP, Brazil

[b] Barcelona University, CPT, Martí I Franqués 1, 08028 Barcelona, Spain

[c] Federal University of Mato Grosso do Sul, P.O. Box 549, 79070-900, Campo Grande, MS, Brazil

*Corresponding author

E-mail address: assis.v.benedetti@unesp.br (A.V. Benedetti)

Abstract

This work describes the morphology, corrosion resistance, and antibacterial performance of copper coating deposited onto carbon steel by cold gas spray (CGS). Cross-sectional images of the coating showed a dense microstructure, with porosity lower than 1%. XRD analysis revealed no oxides or phases different to pure copper. The results of electrochemical tests demonstrated the efficient barrier properties and the compact microstructure of the coating, which protected the substrate against corrosion in chloride solution for more than 1000 h. The copper coating was effective as an antimicrobial agent for inhibiting the growth of *Staphylococcus aureus*, with bacterial growth being completely inhibited after 10 min of direct contact between the bacteria and the coating surface.

Keywords: Metallic coating, cold gas spray, copper, antibacterial surface, *Staphylococcus aureus*.

1. Introduction

Bacterial contamination of the surfaces of materials, especially in public places and hospitals, poses a serious threat [1]. Therefore, huge efforts are made to control infection, aiming at the maximum possible elimination of pathogenic microorganisms, as well as limiting their transfer. The strategies adopted include the use of antimicrobial drugs, hand washing, disinfection, and antibacterial surfaces [1]. On surfaces, many types of microorganisms can persist for long periods of time, with some of them being able to survive for longer than one month [2]. Consequently, surfaces represent a risk in terms of pathogen transmission. In public places and hospitals, some types of components can be manufactured using antimicrobial materials, with the aim of making surfaces self-disinfecting. For this purpose, a recent trend in the management of potentially contaminating environments is to revisit the use of copper alloys or coatings with medical equipment and hospital materials [3].

The mechanism responsible for the antibacterial activity of copper has not yet been completely elucidated [1-10]. However, copper ions released from the copper-containing material are effective in killing bacteria due to the collapse of the outer cell membrane [5]. Copper ions adhere to the bacteria cell surfaces, causing harm to the structure of the proteins [5]. As reported by Grass *et al.* [5, 6, 9, 10], the main factor for obtaining effective antibacterial copper surfaces is a high copper content on the surface. However, the antimicrobial activity diminishes when treatments that decrease the corrosion rate of copper (such as corrosion inhibitors or thick copper oxide layers) are applied [4, 10]. The literature [1-10] has shown that different copper alloys and copper-containing coatings are able to decrease the risk of bacteria emergence and the spread of multi-resistant organisms.

Several coating technologies have been successfully employed with metallic components for antibacterial purposes [7, 8]. Wu *et al.* [7] evaluated the antibacterial performance of Ti-Cu-N coatings deposited onto titanium substrates by magnetron sputtering

with plasma nitriding. The coatings completely killed *S. aureus* after 24 h of contact. Although the Ti-Cu-N coatings showed excellent antibacterial performance, the deposition methodology is expensive and the process is quite long. Goudarzi *et al*. [8] used an atmospheric plasma spraying system to deposit metallic copper coatings onto 316 stainless steel substrates. Analyses showed a microstructure with pores, cracks, and high oxides content. Antibacterial tests showed reduction of *E. coli* and *S. aureus* after 24 h. Although such copper coatings present good antibacterial performance, they are susceptible to severe corrosion, due to the pores and defects in the microstructure, which allow electrolytes to reach the coating/substrate interface. The proportion of copper (antibacterial agent) on the surface is of great importance for antibacterial activity, while the coating thickness and a less porous surface are most important in terms of corrosion and wear resistance performance.

The cold gas spray (CGS) technique is a useful methodology for obtaining surfaces covered by copper, enabling the preparation of thick copper coatings with high adhesion and good resistance to corrosion and wear, at low cost [11-20]. CGS is a solid-state process in which particles are heated below their melting point at temperatures that can vary according to the nozzle design, gas, and spraying parameters used [13, 21-24]. The substrate and particle can be plastically deformed by the impact of the particle, when its velocity exceeds a certain value [13, 25]. The main mechanism postulated for bonding of metals onto metals is adiabatic shear instability (ASI), which occurs when the particle softening overcomes its work hardening [13, 22, 25]. In some cases, the particle shells have been observed to melt, resulting in strong bonds between the coating constituents [13]. As a consequence of the characteristics of the CGS process [25], oxygen-sensitive materials such as aluminum, magnesium, and copper can produce high performance coatings with low residual stress, low oxide formation, and high corrosion resistance [13, 26].

CGS coatings are used in a wide range of industries [14, 22, 24, 27-29] and allow the spraying of different feedstock powders including metals, polymers, composites, and ceramics, with good reproducibility [24, 25]. The coatings have been used as thermal barriers, for corrosion protection, as biomaterials, and in electronic devices [14, 30-34]. In addition, CGS coatings have shown photocatalytic activity [35], antifouling properties [36, 37], and biocompatibility with cells and human tissues [25, 27, 38]. The CGS process improves the performance and functionality of many commercial products, providing them with added value [21-24]. This technique also allows *in situ* repairing of many materials and industrial parts, increasing their lifetimes and decreasing the need for replacements [21-24]. Furthermore, CGS offers the possibility of producing effective coatings without adverse environmental impacts or generation of toxic waste [21-24]. Considering all these positive aspects, the aim of this research was to study the microstructure, corrosion resistance, and antibacterial activity of copper coatings prepared by CGS on carbon steel.

2. Experimental

2.1. Feedstock powders and substrate

The feedstock powder (Cu ≥99%) was produced by gas atomization in an air atmosphere, by Flame Spray Technologies (Duiven, The Netherlands). Laser diffraction spectroscopy (LDS) was used to determine the particle size distribution of the powder. The substrate was a carbon steel alloy with the composition described previously [32]. Flat (5 cm × 2 cm × 0.5 cm) substrates were cleaned with acetone and were then grit blasted using alumina corundum (Al_2O_3, 82±12 μm particle size), which resulted in a surface roughness (Ra) of ~4.7 μm, measured as described elsewhere [32].

2.2 Coatings preparation

The copper coatings were obtained as described previously [39]. The conditions used were a traverse speed of 500 mm/s, standoff distance of 40 mm, nitrogen gas temperature of 400 °C and pressure of 30 bar, and five-layer deposition. Fig. S1 (*SD*) shows the surface of the as-prepared copper coating.

2.3 Structural and morphological analyses

The phase compositions and microstructures of the coatings were investigated by X-ray diffraction (XRD), using a Siemens Model D5000 diffractometer. The morphologies and chemical compositions of the powders and coatings were analyzed by scanning electron microscopy (SEM), using a JEOL JSM-5310 microscope coupled to an X-ray microanalysis (EDS) system. Cross-sectional SEM images (minimum of 10) were analyzed using ImageJ software to determine the mean thickness value. In order to reveal the morphology of the coating surface, the sample was etched using a solution produced with 7 mL H_2O, 3 mL HCl, and 0.3 g $Fe(NO_3)_3$. The surface was analyzed using optical micrographs acquired with a Leica CTR 4000 microscope. Optical images were also used to determine the coating porosity (ASTM E2109-01). Details about the instrumentation used can be found elsewhere [32]. The hardness of the coatings was determined using a Vickers indenter (ASTM E384-99), with mean values obtained from 15 indentations.

2.4 Corrosion measurements

The protection provided by the coating was investigated by recording the E_{OCP} and EIS responses during 120 h (substrate) and 1100 h (copper coating), between 100 kHz and 5 MHz, at 10 mV (rms) *vs.* E_{OCP}. The EIS measurements were performed after 1 h and then at 24-h intervals during the immersion. Further details of the experimental procedure can be found elsewhere [32, 39]. The consistency of the experimental data was evaluated using the

Kramers-Kronig transform (KKT) and electrical equivalent circuit (EEC) fitting was performed with Z-view® software.

2.5 Antibacterial assays

Staphylococcus aureus strain ATCC 25923 was kept at -70 ºC in Müller Hinton broth containing glycerol (20% v/v) (QEEL, São Paulo, Brazil). The bacteria suspension was prepared by adding 40 μL of the bacteria strain to 4 mL of brain heart infusion (BHI) broth and keeping at 37 °C for 24 h. Afterwards, a bacteria solution with turbidity of 0.5 McFarland was prepared, resulting in a concentration of ~1.5 x 10^8 colony-forming units (CFU) per mL.

Prior to the antibacterial assay, all the materials used were autoclaved at 127 °C for 20 min. The coating samples were sonicated in 70% ethyl alcohol for 20 min, placed in Petri dishes, and dried at 37 °C for 30 min. The antibacterial assay was performed by adding 50 μL of bacterial inoculum, at a concentration of 1.5 x 10^8 CFU/mL, to the surfaces of the copper coating and control (glass surface) samples. After spreading the bacteria solution on the surfaces using a sterile spreader, the samples were incubated at 37 °C until being tested for the growth inhibition activity. After the incubation time (0, 5, and 10 min), the sample surfaces were washed with 1000 μL of phosphate buffer saline (PBS) solution at pH 7.3, after which 1 μL of the washing solution was used for plating the bacteria. It should be noted that the incubation time represents the time of contact between the bacteria and the coating surface, so for an incubation time of 0 min, the bacteria solution was spread on the surface, which was then immediately washed. The plate spreading method was used to determine the total bacteria number by counting of the colony-forming units. The assays were performed in triplicate.

3. Results and Discussion

3.1 Structure, morphology and chemical characterization of the powder and coating

The powder showed a micrometric particle size range (20-50 µm), with a mean size of 31±2 µm (Fig. S2, *SD*). The SEM images (Fig. 1) indicated that satellite particles with sizes in the submicron range were formed during solidification in the gas atomization process [41]. The particle morphology was rounded, but not completely spherical, and without pores (Fig. 1). These characteristics confirmed that the feedstock material had ideal size and morphology for being sprayed by CGS. A narrow particle size distribution is desirable, since it results in more uniform particle velocities, while relatively small particles can achieve higher speeds during spraying, hence reaching the substrate with higher kinetic energy, leading to greater plastic deformation and the creation of dense and compact coatings [21, 22]. The XRD pattern of the feedstock powder (Fig. 2) revealed only one phase, which was assigned to copper.

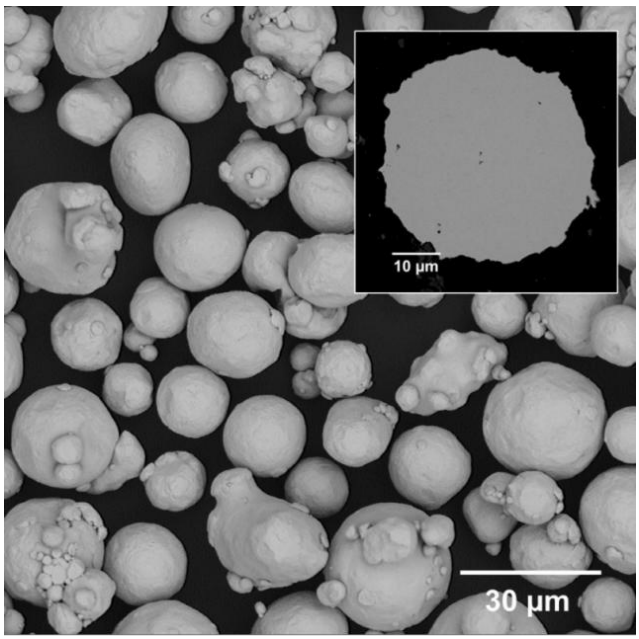

Fig. 1. SEM images showing the surface morphology of the copper feedstock powder and the cross section of a particle (insert).

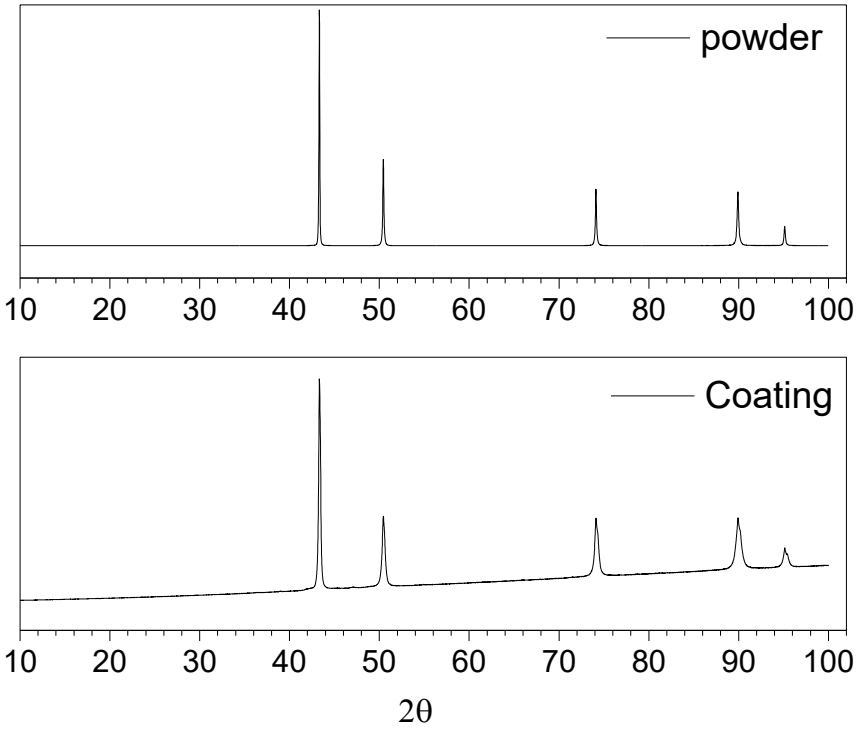

Fig. 2. XRD patterns of the feedstock powder and the coating.

The diffractograms of the coating and the powder showed the same characteristic peaks (Fig. 2). Therefore, the compositions of the feedstock material and the coating were similar, being homogeneous and almost oxide-free. Since CGS is a solid-state deposition technique, the high kinetic and low thermal energies produce coatings with low oxide contents and without fragile phases [25, 26, 43].

The SEM images of the coating cross section (Fig. 3 and Fig. S3, *SD*) revealed a microstructure in which the particles were strongly deformed, without the presence of oxides, cracks, or interconnected porosity [23, 42]. As reported previously [31], the bottom layer of the coating was typically compact, due to the tamping effect of incoming particles, while the top layer was more porous. The dark particles that can be seen at the coating/substrate interface were alumina particles that adhered to the substrate surface during the grit blasting preparation process.

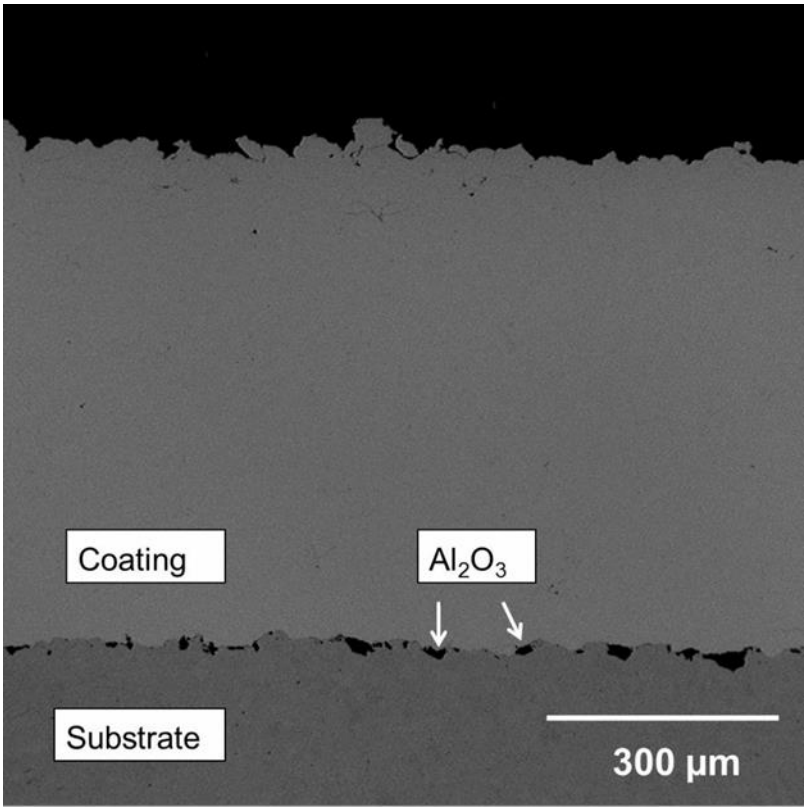

Fig. 3. Cross-sectional SEM image of the copper coating.

The main properties of the copper coating are listed in Table 1. The thickness was 632±11 µm, which was higher than previously reported for copper coatings on carbon steel [44] and other substrates [17, 45]. The porosity was lower than 0.5%, so the copper coating could be considered compact [32, 46]. The adherence of the coating to the substrate was found to be 30 MPa, according to the ASTM C-633 protocol. In the adhesion tests, the coatings failed at the substrate/coating interface, indicating that the interlayer bonding was stronger than that of the substrate-coating interface. The hardness was 147 HV, which was close to the values reported elsewhere [16, 17, 47, 48].

Table 1. Main properties of the copper coating.

Properties	Copper coating
Thickness (μm)	632±11
Porosity (%)	0.5±0.1
Adhesion (MPa)	30±2
Hardness (HV)	147±4

3.2 Corrosion studies

3.2.1 Open circuit potential (E_{OCP}) measurements

The E_{OCP} values for the carbon steel and the coating were determined during 120 h (substrate) and 1100 h (copper coating). In the case of the carbon steel substrate, the E_{OCP} values decreased during the first hours of immersion (Fig. 4), which could be attributed to dissolution of the native oxide film [32, 51]. Oscillations of E_{OCP} were associated with the reaction of chloride ions with the thin oxide layer at the substrate surface, leading to precipitation/dissolution of corrosion products [49, 50]. The potential of the substrate tended to stabilize at ~-0.70 V/Ag|AgCl|$KCl_{3mol/L}$.

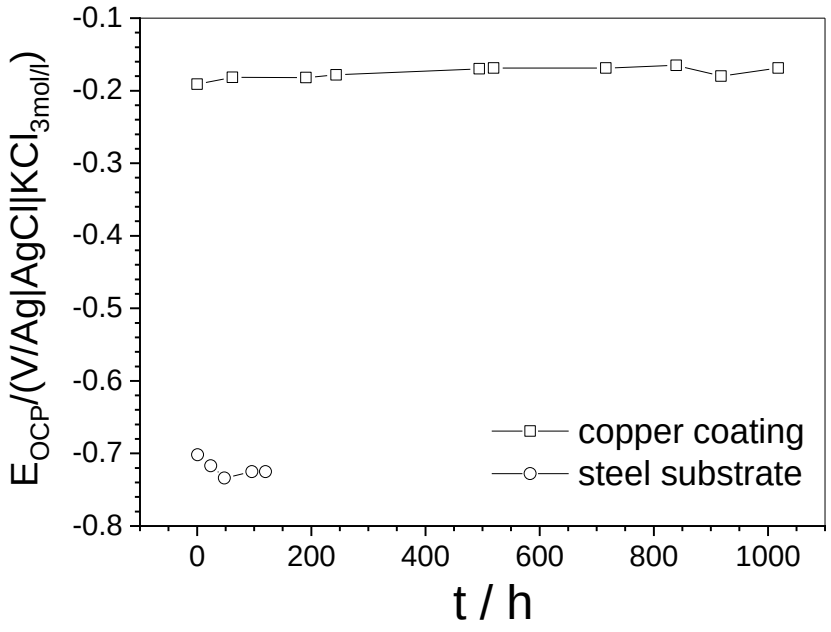

Fig. 4. Plots of E_{OCP}, according to time, for the copper coating and the substrate in 3.5 wt.% NaCl solution, at 25 ºC.

In the case of the copper coating, the E_{OCP} values remained at around -0.2 V/Ag|AgCl|$KCl_{3mol/L}$ throughout the period, as expected for massive copper in chloride solution [52], with oscillations no higher than ±0.05 V. These results indicated that the coating protected the carbon steel from chloride attack for at least 1100 h, due to the barrier effect of the dense copper coating. At the end of the experiment, the cross-sectional SEM image (Fig. 5) and the EDS analyses (Figs. S4 and S5, *SD*) confirmed the integrity of the coating/substrate interface. Only copper was detected near the substrate surface by EDS (Fig. S4, *SD*), corroborating the observed evolution of E_{OCP} with time. Copper oxides were observed at the surface of the coating (Fig. S5, *SD*), but no iron was detected. The EDS analysis is semi-quantitative and therefore only suggested the presence of the oxides, since oxygenated salts cannot be formed in these systems.

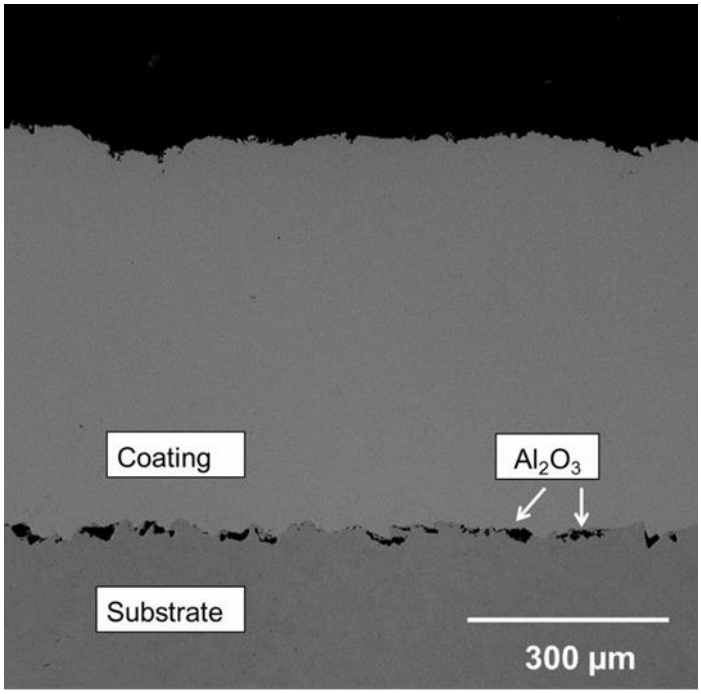

Fig. 5. Cross-sectional SEM image of the copper coating after 1100 h in 3.5 wt.% NaCl.

The detection of copper and oxygen by the EDS analysis suggested that the corrosion mechanism involved the dissolution of copper from the coating, forming cuprous oxide and soluble copper species. The process of copper corrosion in a chloride medium involves a number of steps. Firstly, chloride ions are adsorbed on the copper, according to the reaction [53]:

$$Cu + Cl^- \rightarrow CuCl_{ad} + e^- \quad (1)$$

This adsorbed species has low solubility and can therefore accumulate to form a CuCl film [54-56] and/or react with a chloride ion to form a soluble species [57, 58]:

$$CuCl_{ad} + Cl^- \rightarrow CuCl_2^- \quad (2)$$

It is well known that the CuCl film at the film/solution interface can be partially dissolved to form $CuCl_2^-$ [59, 60], while at [Cl^-] >1 mol/L NaCl, there can be formation of $CuCl_3^{2-}$ and $CuCl_4^{3-}$ complexes, depending on the chloride ion concentration [61]. For example, the following reaction can occur:

$$CuCl_{film} + Cl^- \rightarrow CuCl_2^- \quad (3)$$

On the other hand, in the presence of O_2 and excess of $CuCl_2^-$, the following reaction can take place at the electrode surface [56]:

$$4CuCl_2^- + O_2 + 4H_2O \rightarrow 2Cu_2Cl(OH)_3 + 2H^+ + 4Cl^- \quad (4)$$

Reaction (4) is responsible for the powdery patina of $Cu_2Cl(OH)_3$ on archeological bronzes. The sum of reactions (1) and (2) can also give the following reaction [52]:

$$Cu + 2Cl^- \leftrightarrow CuCl_2^- + e^- \quad (5)$$

In the presence of an excess of $CuCl_2^-$ at the electrode surface and in the absence of O_2, the following reaction has been suggested [56]:

$$2CuCl_2^- + H_2O \leftrightarrow Cu_2O + 4Cl^- + 2H^+ \quad (6)$$

The oxygen reduction is the cathodic reaction during the corrosion of copper and produces predominantly hydroxide groups on the copper surface [63]:

$$O_2 + 2H_2O + 4e^- \rightarrow 4OH^- \quad (7)$$

3.3.2 EIS results

Figs. 6 and 7 show the EIS impedance diagrams for the substrate and coating, respectively, in neutral aerated sodium chloride solution, as a function of time. For the steel substrate, the EIS measurements showed a semicircle in the Nyquist diagrams (Fig. 6a) and one asymmetric time constant, in the medium frequency (MF) range, in the Bode phase angle diagrams (Fig. 6b). The shapes of the Bode phase plots suggested the presence of two time constants, which were discriminated when the experimental data were treated using equivalent electrical circuits (EEC). The semicircle of the complex plane decreased from 48 h to 120 h, suggesting dissolution of the oxide layer and/or desorption of ions [32]. Accordingly, the impedance modulus values also decreased in the low frequency

(LF) range, which could be attributed to iron oxidation and dissolution of the iron oxides porous film [64].

For the copper coating, the complex plane diagrams (Fig. 7a) showed one incomplete and asymmetric semicircle, while the Bode phase angle diagrams (Fig. 7b) showed one asymmetric curve with a maximum at -50° (~200 Hz), which was suggestive of the presence of two overlapping time constants. Two time constants needed to be considered when treating the experimental EIS data.

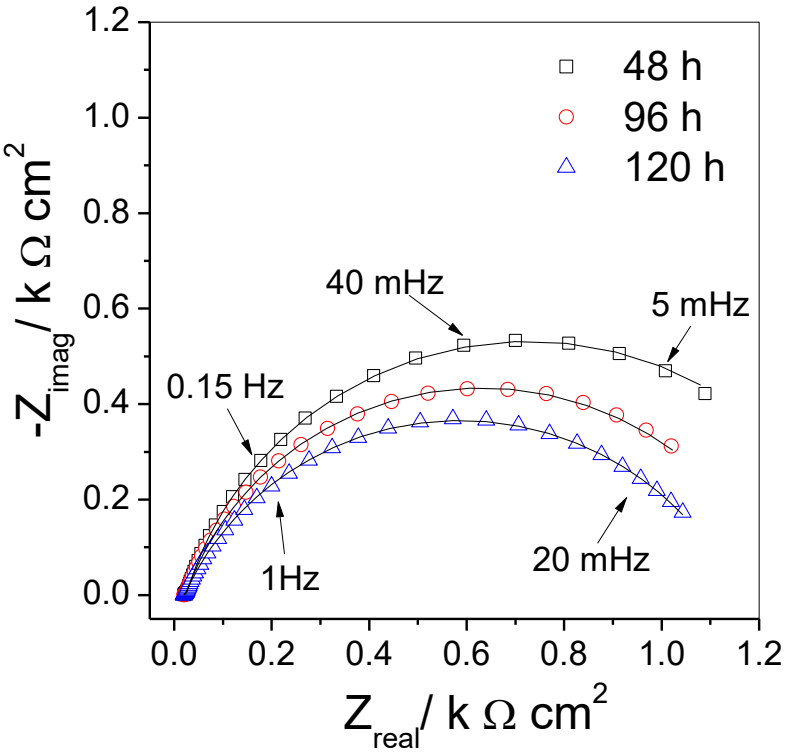

(a)

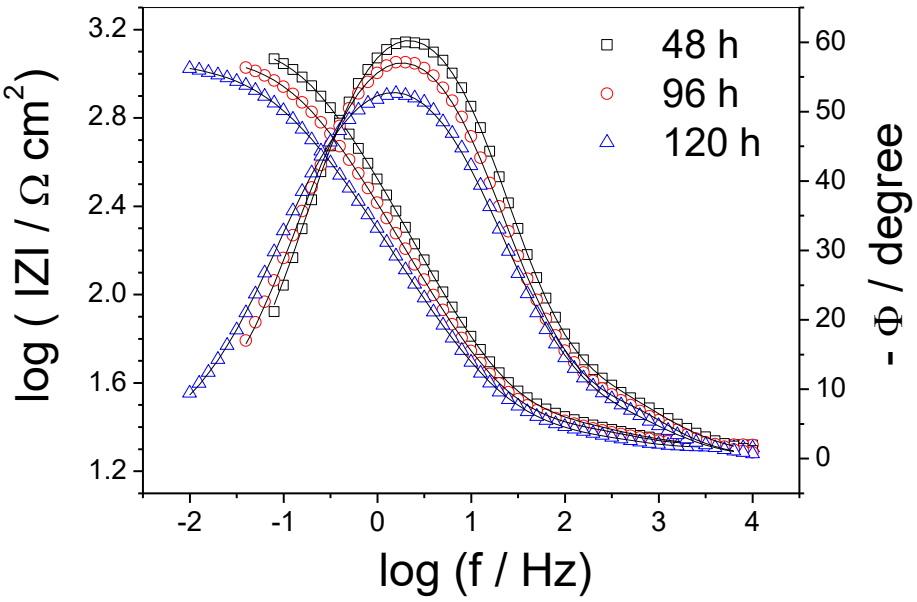

(b)

Fig. 6. (a) Nyquist diagrams and (b) Bode phase diagrams for the substrate in 3.5 wt.% NaCl solution, at 25 °C. The symbols correspond to the experimental data. The fittings are shown by the solid lines.

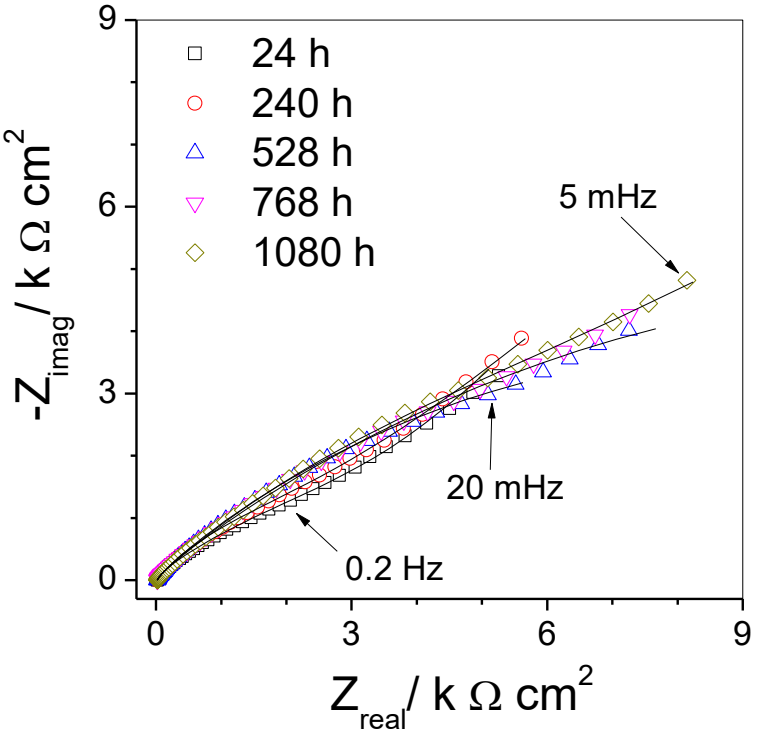

(a)

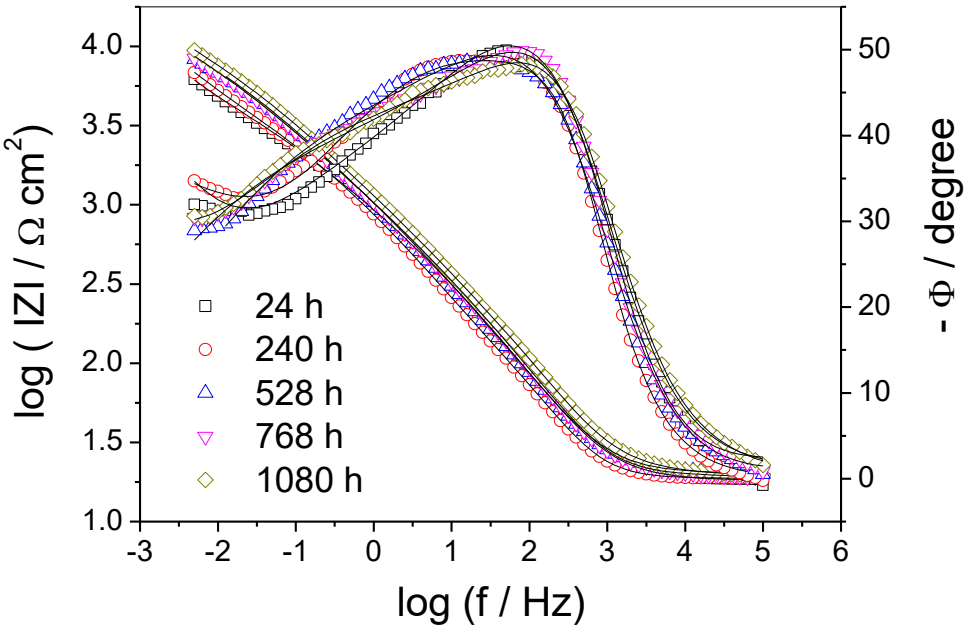

(b)

Fig. 7. (a) Nyquist diagrams and (b) Bode phase diagrams for the copper coating in 3.5 wt.% NaCl solution, at 25 ºC. The symbols correspond to the experimental data. The fittings are shown by the solid lines.

The EIS diagrams were fitted using EECs (Figs. 8 and 9), which were selected based on the microstructures of the coating and the substrate, the quality of the fitting, and the lowest error of each parameter composing the EECs (Table S1, *SD*). The EEC shown in Fig. 8a was used to fit the substrate data. The time constant at MF was described by the $CPE_{dl}//R_{ct}$ sub-circuit attributed to oxygen reduction and iron oxidation, where CPE_{dl} is the constant phase element proportional to the capacitance of the electrical double layer, and R_{ct} is the charge transfer resistance. The data at LF were described by the CPE_{film}/R_{film} sub-circuit attributed to formation/dissolution of a non-protective iron-based film, with desorption of iron ions. The CPE_{film} element is the constant phase element associated with the capacitance of the

film (adsorbed species and iron oxides-hydroxides), while the R_{film} element is associated with the resistance of the film and the electrolyte inside the defects and pores of the film [32].

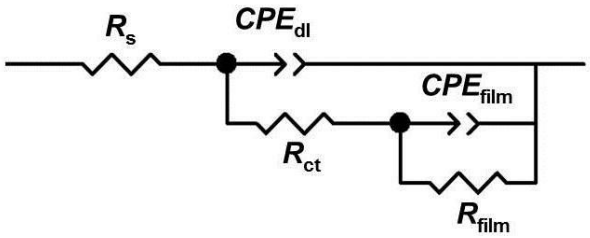

Fig. 8. Electrical equivalent circuit used to fit the EIS data for the substrate.

Fig. 9 shows the scheme used to represent the coating and the corresponding electrical equivalent circuits used to fit the EIS data obtained at different immersion times. The coating was composed of a porous upper layer with defects, together with a compact layer at the bottom, as observed in the SEM images (Fig. 2 and Fig. S5, *SD*). The oxidation of copper in chloride solution occurs within short time intervals and at HF-MF frequencies (Fig. 9a). The corresponding time constant is described by the $CPE_{dl}//R_{ct}$ sub-circuit. The localized dissolution of copper in some regions created the pores, whose electrochemical response was fitted by the $CPE_{po}//R_{po}$ sub-circuit related to the response of the solution inside the pores [65-70]. The pores were formed due to the dissolution of copper at specific sites [32, 46, 71-78], as well as at some defects of the coatings (Fig. 5). For immersion times longer than 630 h, the following features were considered for selection and justification of the EECs: (a) cross-sectional SEM images (Fig. 5) and EDS results (Figs. S5 and S6, *SD*), obtained after long immersion times, which showed no corrosion at the coating/substrate interface; (b) the E_{OCP} remained constant at ~-0.20 V/Ag|AgCl|$KCl_{3mol/L}$ for the entire duration of the test (Fig. 4), indicating that the coating/substrate interface was not reached by the electrolyte; and (c) the pores became deeper, but did not reach the coating/substrate interface.

Based on the observations described previously for the system at t ≥630 h and for quantitative treatment of the EIS data, a third time constant (CPE_{bott}//R_{bott}) was required to fit the impedance diagrams. This time constant was assigned to the capacitance and to the charge transfer resistance due to the copper oxidation reaction at the bottom of pores, where some corrosion products could accumulate.

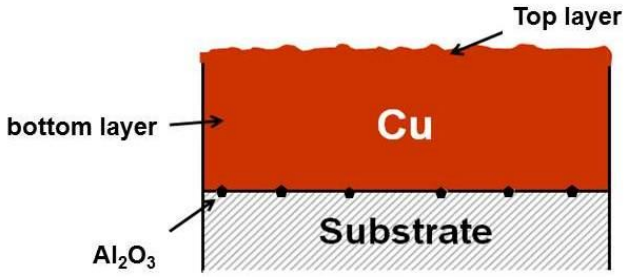

(a)

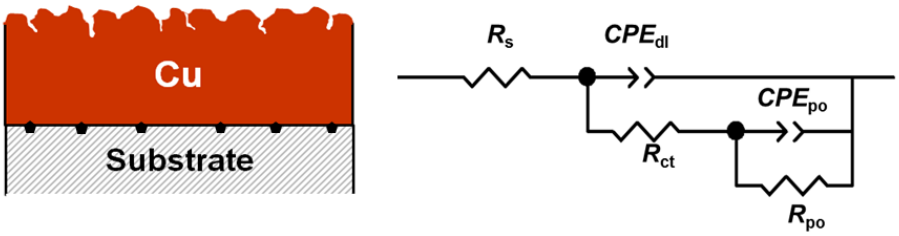

t ≤ 528 h

(b)

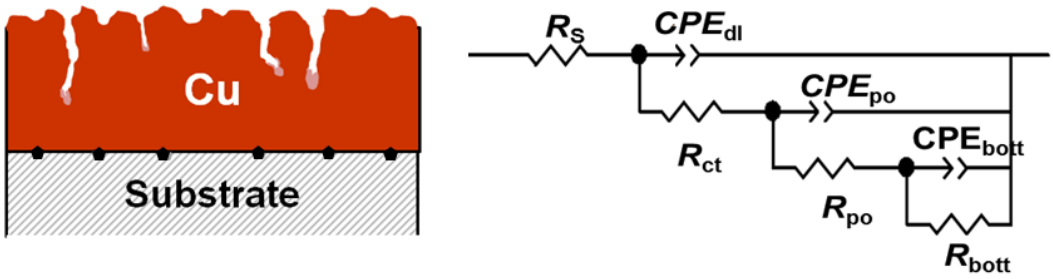

t ≥ 630 h

(c)

Fig. 9. Scheme representing the coatings before (a) and after (b and c) different times of immersion, and the EECs used to fit the impedance diagrams.

Table S1 (*SD*) and Fig. 10 show the evolution of the R_{ct} and R_{po} values, according to the immersion time. For the copper coating, the R_{ct} value remained at 140 Ω cm^2 until 100 h of immersion, after which it abruptly decreased to 40 Ω cm^2 and remained steady near this value until the end of the experiment. At the beginning of the test, the coating surface presented a native copper oxide film with defects, which was responsible for the high charge transfer resistance values. Since this oxide layer was attacked by chloride, its resistance decreased, which exposed copper to the solution and led to an abrupt decrease of the R_{ct} values. The R_{po} values oscillated between 1 and 5 kΩ cm^2 for immersion times from 1 h to 600 h. For t >600 h, R_{po} increased to ~120 kΩ cm^2 and remained close to this value until the end of the experiment. The oscillations of R_{po} could have been associated with the number, size, and depth of pores, until reaching certain values. The n_{po} values were around 0.5 during this time interval, which could be attributed to the diffusion of oxygen, chloride ions, or products of copper corrosion through the pores.

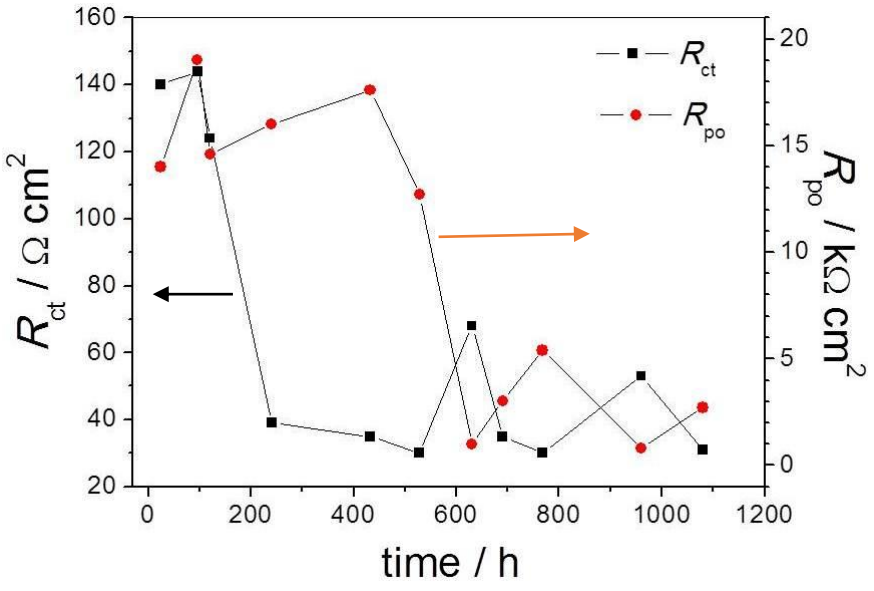

Fig. 10. Values of R_{ct} and R_{po}, according to time, for the copper coating in 3.5% NaCl solution, at 25 °C.

At 630 h, a third time constant, R_{bott}, was added in order to fit the experimental data (Table S1, *SD*). The R_{bott} value at 630 h was 11 kΩ cm^2 and then remained at 12±1 kΩ cm^2 up to 1100 h. The oscillation of R_{bott} could be explained by the growth and dissolution of the corrosion products at the bottom of the pores.

3.3.3 Antibacterial assay

The antibacterial activity of the copper coating was determined using the plate count method. Representative images of bacteria colonies in the Petri dishes at 0, 5, and 10 min of the contact test are shown in Fig. 11. The results showed that the copper surface coating was able to successfully inactivate *Staphylococcus aureus* after a few minutes of contact. There was a 2 orders of magnitude inhibition of bacterial growth after the first 5 min of contact, followed by complete mortality of the bacteria after 10 min. In contrast, no inhibition of bacterial growth was observed for the control (a glass surface), demonstrating that the experimental conditions permitted normal growth of the bacteria. Fig. 12 shows the results of quantitative analyses of the growth response of *Staphylococcus aureus*. The growth of the bacteria decreased from 1.97×10^8 to 0.97×10^6 CFU/mL (by ~2 orders of magnitude) after 5 min, while 100% inhibition of bacterial growth was observed after 10 min. Therefore, the copper coating presented high antibacterial activity against *Staphylococcus aureus*. As described previously, the surface of this coating was almost oxide-free (Fig. 3 and Fig. S4, *SD*), which allowed direct contact between the metal surface and the bacteria. In contact with humidity and bacteria, the metallic copper on the coating surface was oxidized to copper ions, which were responsible for destroying the cell walls of the bacteria and inhibiting their

growth [79, 80]. As mentioned above, it is also possible that the released Cu ions caused collapse of the outer cell membranes, killing the bacteria or damaging the structure of proteins, as a consequence of adhesion of the ions to the surfaces of the cells [5, 80]. Therefore, the quantity of copper ions released, which was directly related to the dissolution of copper from the coating, determined the antibacterial activity [5].

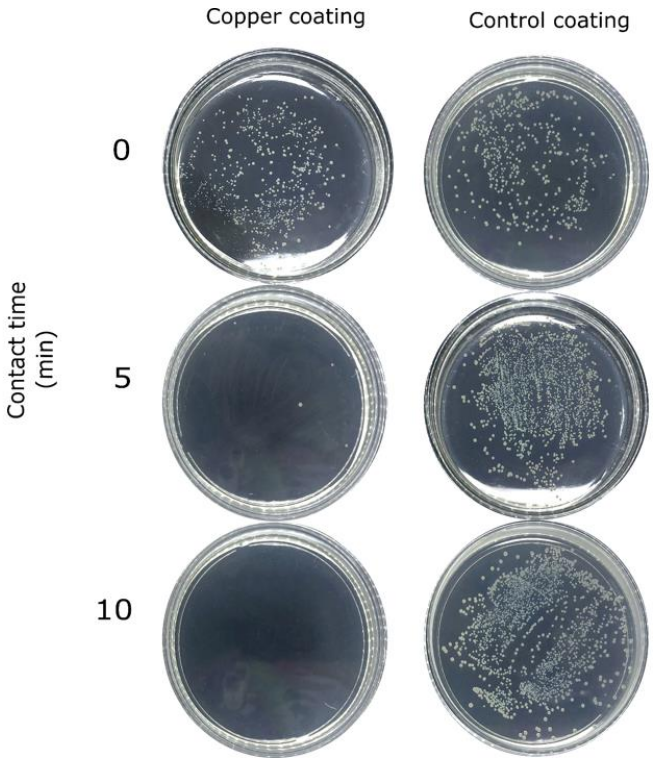

Fig. 11. Growth of *Staphylococcus aureus* colonies in Petri dishes after 24 h at ~25 °C.

The copper coatings deposited by CGS showed higher antibacterial efficiency against *Staphylococcus aureus*, compared to other antibacterial surfaces [10, 81, 82]. Xiang-Yu *et al*. [81] reported that stainless steel covered by a copper layer showed complete inhibition of *Staphylococcus aureus* growth after 3 h. In other work, brass (20 wt.% Zn and 80 wt.% Cu) caused a reduction of *Staphylococcus aureus* growth after 6 h, without complete inhibition [82]. Therefore, the CGS technique was able to produce antibacterial copper surfaces that offered higher performance.

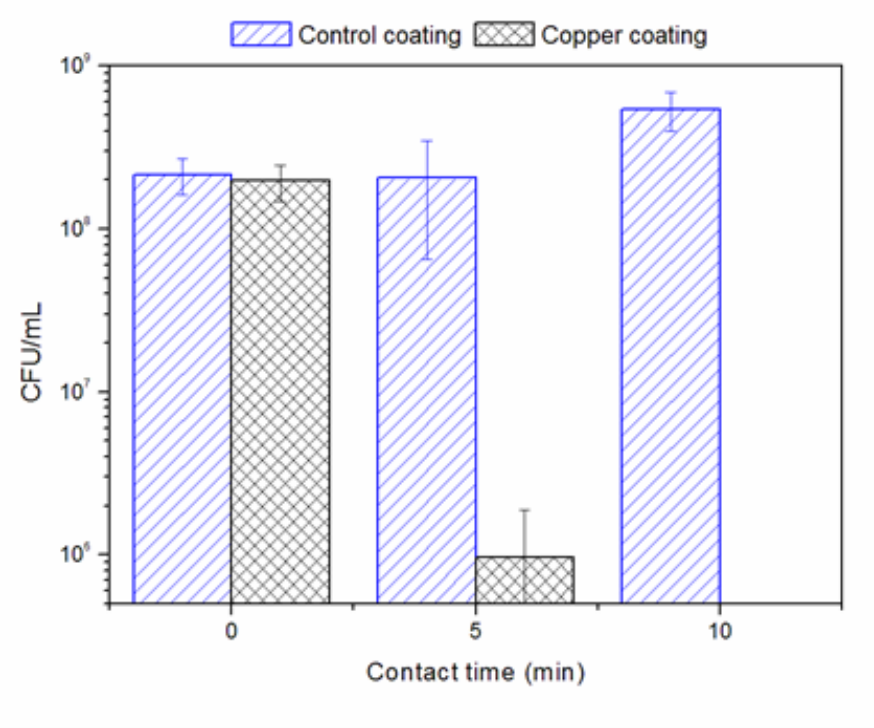

Fig. 12. Mean CFU values for *Staphylococcus aureus* after different times of exposure to the copper coating. After 10 min, no bacteria colonies were found on the copper surface.

4. Conclusions

In this study, the cold gas spray method produced copper coatings with excellent corrosion resistance and high antibacterial activity. The dense microstructure, high thickness, and low porosity improved the barrier effect of the copper coating and enabled protection of carbon steel against corrosion for ~1100 h of immersion in chloride solution. No corrosion was detected at the coating/substrate interface after ~1100 h, due to the compactness of the coating obtained by cold gas spray. The results of antibacterial assays showed that the copper coating presented strong antibacterial activity against *Staphylococcus aureus*, with 100% mortality of the bacteria after 10 min.

5. Acknowledgements

The authors thank CNPq (Conselho Nacional de Pesquisa, procs. 153177/2014-4 and 201325/2014-4), CAPES (Coordenação de Aperfeiçoamento do Pessoal de Ensino Superior), and Fundect (Fundação de Apoio ao Desenvolvimento do Ensino, Ciência e Tecnologia do Estado de Mato Grosso do Sul, proc. 59/300.490/2016) for financial support and scholarships.

6. References

[1] A. Mikolay, S. Huggett, L. Tikana, G. Grass, J. Braun, D. H. Nies, Survival of bacteria on metallic copper surfaces in a hospital trial, Appl. Microbiol. Biotechnol. 87 (2010) 1875–1879. doi:10.1007/s00253-010-2640-1.

[2] A. Kramer, I. Schwebke, G. Kampf, How long do nosocomial pathogens persist on inanimate surfaces? A systematic review, BMC Infect. Dis. 6 (2006) 130-138. doi:10.1186/1471-2334-6-130.

[3] R. B. Thurman, C. P. Gerba, G. Bitton, The molecular mechanisms of copper and silver ion disinfection of bacteria and viruses, Crit. Rev. Environ. Control. 18 (1989) 295–315. doi:10.1080/10643388909388351.

[4] J. Zhao, D. Xu, M. B. Shahzad, Q. Kang, Y. Sun, Z. Sun, S. Zhang, L. Ren, C. Yang, K. Yang, Effect of surface passivation on corrosion resistance and antibacterial properties of Cu-bearing 316L stainless steel, Appl. Surf. Sci. 386 (2016) 371–380. doi:10.1016/j.apsusc.2016.06.036.

[5] T. Xi, M. B. Shahzad, D. Xu, Z. Sun, J. Zhao, C. Yang, M. Qi, K. Yang, Effect of copper addition on mechanical properties, corrosion resistance and antibacterial property of 316L stainless steel, Mater. Sci. Eng. C 71 (2017) 1079–1085. doi:10.1016/j.msec.2016.11.022.

[6] H. Chai, L. Guo, X. Wang, Y. Fu, J. Guan, L. Tan, L. Ren, K. Yang, Antibacterial effect of 317L stainless steel contained copper in prevention of implant-related infection in vitro and in vivo, J. Mater. Sci. Mater. Med. 22 (2011) 2525–2535. doi:10.1007/s10856-011-4427-z.

[7] H. Wu, X. Zhang, X. He, M. Li, X. Huang, R. Hang, B. Tang, Wear and corrosion resistance of anti-bacterial Ti–Cu–N coatings on titanium implants, Appl. Surf. Sci. 317 (2014) 614–621.

[8] M. Goudarzi, S. Saviz, M. Ghoranneviss, A. Salar Elah, Medical equipment antiseptic processes using the atmospheric plasma sprayed copper coatings, J. X-ray Sci. Technol. 25 (3) (2017) 479-485. doi: 10.3233/XST-16194.

[9] G. Faúndez, M. Troncoso, P. Navarrete, G. Figueroa, Antimicrobial activity of copper surfaces against suspensions of Salmonella enterica and Campylobacter jejuni, BMC Microbiol. 4 (2004) 19-26. doi:10.1186/1471-2180-4-19.

[10] G. Grass, C. Rensing, M. Solioz. Metallic Copper as an Antimicrobial Surface, Appl. Environ. Microbiol. 77 (2011) 1541–1547. doi:10.1128/AEM.02766-10.

[11] T. Klassen, F. Gärtner, T. Schmidt, J. O. Kliemann, K. Onizawa, K. R. Donner, H. Gutzmann, K. Binder, H. Kreye, Basic principles and application potentials of cold gas spraying, Materwiss Werksttech. 41 (2010) 575–584. doi:10.1002/mawe.201000645.

[12] E. Irissou, J. Legoux, A. N. Ryabinin, B. Jodoin, C. Moreau, Review on Cold Spray Process and Technology : Part I — Intellectual Property, J. Therm. Spray Technol. 17 (2008) 495–516. doi:10.1007/s11666-008-9203-3.

[13] N. Bala, H. Singh, J. Karthikeyan, S. Prakash, Cold spray coating process for corrosion protection: a review, Surf. Eng. 30 (2014) 414–421. doi:10.1179/1743294413Y.0000000148.

[14] H. Singh, T. S. Sidhu, S. B. S. Kalsi, J. Karthikeyan, Development of cold spray from innovation to emerging future coating technology, J. Brazilian Soc. Mech. Sci. Eng. 35 (2013) 231–245. doi:10.1007/s40430-013-0030-1.

[15] S. Grigoriev, A. Okunkova, A. Sova, P. Bertrand, I. Smurov, Cold spraying: From process fundamentals towards advanced applications, Surf. Coatings Technol. 268 (2014) 77–84. doi:10.1016/j.surfcoat.2014.09.060.

[16] P. Sudharshan Phani, D. Srinivasa Rao, S. V. Joshi, G. Sundararajan, Effect of Process Parameters and Heat Treatments on Properties of Cold Sprayed Copper Coatings, J. Therm. Spray Technol. 16 (2007) 425–434. doi:10.1007/s11666-007-9048-1.

[17] K. I. Triantou, D. I. Pantelis, V. Guipont, M. Jeandin, Microstructure and tribological behavior of copper and composite copper+alumina cold sprayed coatings for various alumina contents, Wear 336–337 (2015) 96–107. doi:10.1016/J.WEAR.2015.05.003.

[18] T. Kairet, M. Degrez, F. Campana, J. Janssen, Influence of the Powder Size Distribution on the Microstructure of Cold-Sprayed Copper Coatings Studied by X-ray Diffraction, J. Therm. Spray Technol. 16 (2007) 610–618. doi:10.1007/s11666-007-9116-6.

[19] F. Gärtner, T. Stoltenhoff, J. Voyer, H. Kreye, S. Riekehr, M. Koçak, Mechanical properties of cold-sprayed and thermally sprayed copper coatings, Surf. Coatings Technol. 200 (2006) 6770–6782. doi:10.1016/J.SURFCOAT.2005.10.007.

[20] L. Venkatesh, N. M. Chavan, G. Sundararajan, The Influence of Powder Particle Velocity and Microstructure on the Properties of Cold Sprayed Copper Coatings, J. Therm. Spray Technol. 20 (2011) 1009–1021. doi:10.1007/s11666-011-9614-4.

[21] V. K. Champagne, The cold spray materials deposition process Fundamentals and applications (2007). ISBN: 9781845693787

[22] F. S. da Silva, N. Cinca, S. Dosta, I. G. Cano, A. V. Benedetti, J. M. Guilemany, Cold gas

spray coatings: basic principles corrosion protection and applications, Eclét. Quím. J. 42 (2017) 09-32. doi:10.26850/1678-4618eqj.v42.1.2017.p09-32.

[23] R. N. Raoelison, Y. Xie, T. Sapanathan, M. P. Planche, R. Kromer, S. Costil, C. Langlade, Cold gas dynamic spray technology: A comprehensive review of processing conditions for various technological developments till to date, Addit. Manuf. 19 (2018) 134–159.
doi:10.1016/J.ADDMA.2017.07.001.

[24] R. N. Raoelison, Ch. Verdy, H. Liao, Cold gas dynamic spray additive manufacturing today: Deposit possibilities, technological solutions and viable applications, Mater. Des. 133 (2017) 266–287. doi:10.1016/J.MATDES.2017.07.067.

[25] A. Moridi, S. M. Hassani-Gangaraj, M. Guagliano, M. Dao, Cold spray coating: review of material systems and future perspectives, Surf. Eng. 30 (2014) 369–395. doi:10.1179/1743294414Y.0000000270.

[26] B. Jodoin, L. Ajdelsztajn, E. Sansoucy, A. Zúñiga, P. Richer, E. J. Lavernia, Effect of particle size, morphology, and hardness on cold gas dynamic sprayed aluminum alloy coatings, Surf. Coatings Technol. 201 (2006) 3422–3429. doi:10.1016/j.surfcoat.2006.07.232.

[27] J. Villafuerte, Applications, in: Modern Cold Spray, Springer (2015). ISBN 9783319167725.

[28] L. Pawlowski, The Science and Enginnering of Thermal Spray Coatings, second edition (2008). ISBN 978-0-471-49049-4

[29] A. Sova, S. Grigoriev, A. Okunkova, I. Smurov, Potential of cold gas dynamic spray as additive manufacturing technology, Int. J. Adv. Manuf. Technol. 69 (2013) 2269–2278. doi:10.1007/s00170-013-5166-8.

[30] R. M. Souto, M. M. Laz, R. L. Reis, Degradation characteristics of hydroxyapatite coatings on orthopaedic TiAlV in simulated physiological media investigated by electrochemical impedance spectroscopy, Biomaterials 24 (2003) 4213–4221. doi:10.1016/S0142-9612(03)00362-4.

[31] X. Zhou, P. Mohanty, Electrochemical behavior of cold sprayedhydroxyapatite/titanium composite in Hanks' solution, Electrochim. Acta. 65 (2012) 134–140. doi:10.1016/j.electacta.2012.01.018.

[32] F. S. da Silva, J. Bedoya, S. Dosta, N. Cinca, I.G. Cano, J. M. Guilemany, A. V. Benedetti, Corrosion characteristics of cold gas spray coatings of reinforced aluminum deposited onto carbon steel, Corros. Sci. 114 (2017) 57-71. doi:10.1016/j.corsci.2016.10.019.

[33] A. M. Vilardell, N. Cinca, A. Concustell, S. Dosta, I. G. Cano, J. M. Guilemany, Cold spray as an emerging technology for biocompatible and antibacterial coatings: state of art, J. Mater. Sci. 50 (2015) 4441–4462. doi:10.1007/s10853-015-9013-1.

[34] N. Cinca, A. M. Vilardell, S. Dosta, A. Concustell, I. Garcia Cano, J. M. Guilemany, S. Estradé, A. Ruiz, F. Peiró, A New Alternative for Obtaining Nanocrystalline Bioactive Coatings: Study of Hydroxyapatite Deposition Mechanisms by Cold Gas Spraying, J. Am. Ceram. Soc. 99 (2016) 1420–1428. doi:10.1111/jace.14076.

[35] M. Robotti, S. Dosta, C. Fernández-Rodríguez, M. J. Hernández-Rodríguez, I. G. Cano, E. P. Melián, J. M. Guilemany, Photocatalytic abatement of NOx by C-TiO_2/polymer composite coatings obtained by low pressure cold gas spraying, Appl. Surf. Sci. 362 (2016) 274–280. doi:10.1016/j.apsusc.2015.11.207.

[36] C. Stenson, K. A. McDonnell, S. Yin, B. Aldwell, M. Meyer, D. P. Dowling, R. Lupoi, Cold spray deposition to prevent fouling of polymer surfaces, Surf. Eng. Journal 34 (3) (2018) 1-11. doi:10.1080/02670844.2016.1229833

[37] M. J. Vucko, P.C. King, A. J. Poole, Y. Hu, M. Z. Jahedi, R. de Nys, Assessing the antifouling properties of cold-spray metal embedment using loading density gradients of metal particles., Biofouling. 30 (2014) 651–666. doi:10.1080/08927014.2014.906584.

[38] A. M. Vilardell, N. Cinca, I. G. Cano, A. Concustell, S. Dosta, J. M. Guilemany, S.

Estradé, A. Ruiz-Caridad, F. Peiró, Dense nanostructured calcium phosphate coating on titanium by cold spray, J. Eur. Ceram. Soc. 37 (2017) 1747–1755. doi:10.1016/j.jeurceramsoc.2016.11.040.

[39] F. S. da Silva, K. Zomeño, S. Dosta, N. Cinca, I. G. Cano, J. M. Guilemany, A. V. Benedetti, Influence of different copper feedstock powders on the microstructure and corrosion of coatings prepared by cold gas spray, Corros. Sci. (2018) in revision.

[40] W.S. Tait, An introduction to electrochemical corrosion testing for practicing engineers and scientists., Wisconsin Pair Odocs, 1994.

[41] S. Lagutkin, L. Achelis, S. Sheikhaliev, V. Uhlenwinkel, V. Srivastava, Atomization process for metal powder, Mater. Sci. Eng. A. 383 (2004) 1–6. doi:10.1016/j.msea.2004.02.059.

[42] M. M. Sharma, T. J. Eden, B. T. Golesich, Effect of Surface Preparation on the Microstructure, Adhesion, and Tensile Properties of Cold-Sprayed Aluminum Coatings on AA2024 Substrates, J. Therm. Spray Technol. 24 (2014) 410–422. doi:10.1007/s11666-014-0175-1.

[43] K. Balani, T. Laha, A. Agarwal, J. Karthikeyan, N. Munroe, Effect of carrier gases on microstructural and electrochemical behavior of cold-sprayed 1100 aluminum coating, Surf. Coatings Technol. 195 (2005) 272–279. doi:10.1016/j.surfcoat.2004.06.028.

[44] W. Y. Li, C. J. Li, H. Liao, Significant influence of particle surface oxidation on deposition efficiency, interface microstructure and adhesive strength of cold-sprayed copper coatings, Appl. Surf. Sci. 256 (2010) 4953–4958. doi:10.1016/j.apsusc.2010.03.008.

[45] M. Yu, W. Li, X. Guo, H. Liao, Impacting Behavior of Large Oxidized Copper Particles in Cold Spraying, J. Therm. Spray Technol. 22 (2013) 433–440. doi:10.1007/s11666-012-9849-8.

[46] F. S. da Silva, N. Cinca, S. Dosta, I. G. Cano, M. Couto, J. M. Guilemany, A. V.

Benedetti, Corrosion behavior of WC-Co coatings deposited by cold gas spray onto AA 7075-T6, Corros. Sci. 136 (2018) 231-243. doi:10.1016/J.CORSCI.2018.03.010.

[47] S. Yin, X. Wang, X. Suo, H. Liao, Z. Guo, W. Li, C. Coddet, Deposition behavior of thermally softened copper particles in cold spraying, Acta Mater. 61 (2013) 5105–5118. doi:10.1016/j.actamat.2013.04.041.

[48] E. Calla, D. G. McCartney, P. H. Shipway, Effect of Deposition Conditions on the Properties and Annealing Behavior of Cold-Sprayed Copper, J. Therm. Spray Technol. 15 (2006) 255–262. doi:10.1361/105996306X108192.

[49] J. M. Guilemany, J. Fernandez, J. Delgado, A. V. Benedetti, F. Climent, Effects of thickness coating on the electrochemical behaviour of thermal spray Cr3C2–NiCr coatings, Surf. Coatings Technol. 153 (2002) 107–113. doi:10.1016/S0257-8972(01)01679-6.

[50] J. M. Guilemany, J. Fernández, J. Delgado, Electrochemical measurements and characterisation of a thermally sprayed HVOF Cr_3C_2–NiCr coating in a corrosive environment, Proc. ITSC Düsseldorf, Ger. (1999) 474–478.

[51] J.-D. Kim, S.-I. Pyun, The effects of applied potential and chloride ion on the repassivation kinetics of pure iron, Corros. Sci. 38 (1996) 1093–1102. doi:10.1016/0010-938X(96)00004-2.

[52] W. A. Badawy, K. M. Ismail, A. M. Fathi, Effect of Ni content on the corrosion behavior of Cu-Ni alloys in neutral chloride solutions, Electrochim. Acta. 50 (2005) 3603–3608. doi:10.1016/j.electacta.2004.12.030.

[53] J.-P. Diard, J.-M. Le Canut, B. Le Gorrec, C. Montella, Copper electrodissolution in 1M HCl at low current densities. I. General steady-state study, Electrochim. Acta. 43 (1998) 2469–2483. doi:10.1016/S0013-4686(97)10155-4.

[54] H. P. Lee, K. Nobe, A. J. Pearlstein, Film Formation and Current Oscillations in the

Electrodissolution of Cu in Acidic Chloride Media, J. Electrochem. Soc. 132 (1985) 1031-1037. doi:10.1149/1.2114010.

[55] C.I. Elsner, R. C. Salvarezza, A. J. Arvia, The influence of halide ions at submonolayer levels on the formation of oxide layer and electrodissolution of copper in neutral solutions, Electrochim. Acta. 33 (1988) 1735–1741. doi:10.1016/0013-4686(88)85008-4.

[56] F. K. Crundwell, The anodic dissolution of 90% copper-10% nickel alloy in hydrochloric acid solutions, Electrochim. Acta. 36 (1991) 2135–2141. doi:10.1016/0013-4686(91)85221-R.

[57] A. V. Benedetti, P. T. A. Sumodjo, K. Nobe, P. L. Cabot, W. G. Proud, Electrochemical studies of copper, copper-aluminium and copper-aluminium-silver alloys: Impedance results in 0.5M NaCl, Electrochim. Acta. 40 (1995) 2657–2668. doi:10.1016/0013-4686(95)00108-Q.

[58] G. Kear, B. D. Barker, K. Stokes, F. C. Walsh, Electrochemical Corrosion Behaviour of 90–10 Cu–Ni Alloy in Chloride-Based Electrolytes, J. Appl. Electrochem. 34 (2004) 659–669. doi:10.1023/B:JACH.0000031164.32520.58.

[59] A. K. Hauser, J. Newman, Singular Perturbation Analysis of the Faradaic Impedance of Copper Dissolution Accounting for the Effects of Finite Rates of a Homogeneous Reaction, J. Electrochem. Soc. 136 (1989) 2820-2831. doi:10.1149/1.2096293.

[60] O. E. Barcia, O. R. Mattos, N. Pebere, B. Tribollet, Mass-Transport Study for the Electrodissolution of Copper in 1M Hydrochloric Acid Solution by Impedance, J. Electrochem. Soc. 140 (1993) 2825-2832. doi:10.1149/1.2220917.

[61] K. Nobe, G. L. Bauerle, Technical Note: Effects of Chloride Ions on the Anodic Dissolution of 90/10 and 70/30 Cu-Ni Alloys in H_2SO_4, Corrosion 37 (1981) 426–427. doi:10.5006/1.3578205.

[62] J. Wang, C. Xu, G. Lv, Formation processes of CuCl and regenerated Cu crystals on

bronze surfaces in neutral and acidic media, Appl. Surf. Sci. 252 (2006) 6294–6303. doi:10.1016/j.apsusc.2005.08.041.

[63] D. Wang, B. Xiang, Y. Liang, S. Song, C. Liu, Corrosion control of copper in 3.5 w.% NaCl Solution by Domperidone: Experimental and Theoretical Study, Corros. Sci. 85 (2014) 77–86. doi:10.1016/j.corsci.2014.04.002.

[64] H. C. Kuo, K. Nobe, Electrodissolution kinetics of iron in chloride solution. VI. Concentrated acidic solutions, J. Electrochem. Soc. 125 (1978) 853–860. doi:10.1149/1.2131567.

[65] K. Rahmouni, M. Keddam, A. Srhiri, H. Takenouti, Corrosion of copper in 3% NaCl solution polluted by sulphide ions, Corros. Sci. 47 (2005) 3249–3266. doi:10.1016/j.corsci.2005.06.017.

[66] J.-P. Diard, J.-M. Le Canut, B. Le Gorrec, C. Montella, Copper electrodissolution in 1M HCl at low current densities. II. Electrochemical impedance spectroscopy study, Electrochim. Acta. 43 (1998) 2485–2501. doi:10.1016/S0013-4686(97)10156-6.

[67] E. M. Sherif, S.-M. Park, Inhibition of Copper Corrosion in 3.0% NaCl Solution by NPhenyl-1,4-phenylenediamine, J. Electrochem. Soc. 152 (2005) B428-B433. doi:10.1149/1.2018254.

[68] T. Tüken, B. Yazıcı, M. Erbil, B. Yazici, M. Erbil, The use of polyindole for prevention of copper corrosion, Surf. Coatings Technol. 200 (2006) 4802–4809. doi:10.1016/j.surfcoat.2005.04.023.

[69] A. M. Fenelon, C. B. Breslin, The electrochemical synthesis of polypyrrole at a copper electrode: Corrosion protection properties, Electrochim. Acta. 47 (2002) 4467–4476. doi:10.1016/S0013-4686(02)00518-2.

[70] W.J. Lorenz, Der einfluss von halogenidionen auf die anodische auflösung des eisens, Corros. Sci. 5 (1965) 121–131. doi:10.1016/S0010-938X(65)90478-6.

[71] Y. Bai, Z. H. Wang, X. B. Li, G. S. Huang, C. X. Li, Y. Li, Corrosion behavior of low pressure cold sprayed Zn-Ni composite coatings, J. Alloys Compd. 719 (2017) 194–202. doi:10.1016/j.jallcom.2017.05.134.

[72] Y. Van Ingelgem, A. Hubin, J. Vereecken, Investigation of the first stages of the localized corrosion of pure copper combining EIS, FE-SEM and FE-AES, Electrochim. Acta. 52 (2007) 7642–7650. doi:10.1016/j.electacta.2006.12.039.

[73] R. Babić, M. Metikoš-Huković, A. Jukić, A Study of Copper Passivity by Electrochemical Impedance Spectroscopy, J. Electrochem. Soc. 148 (2001) B146–B151. doi:10.1149/1.1354608.

[74] B. Rosborg, J. Pan, An electrochemical impedance spectroscopy study of copper in a bentonite/saline groundwater environment, Electrochim. Acta. 53 (2008) 7556–7564. doi:10.1016/j.electacta.2008.04.021.

[75] Y. Feng, K.S. Siow, W.K. Teo, K.L. Tan, A.K. Hsieh, Corrosion Mechanisms and Products of Copper in Aqueous Solutions at Various pH Values, Corrosion 53 (1997) 389–398. doi:10.5006/1.3280482.

[76] I. Betova, B. Beverskog, M. Bojinov, P. Kinnunen, K. Mäkelä, S.-O. Pettersson, T. Saario, Corrosion of copper in simulated nuclear waste repository conditions, Electrochem. Solid-State Lett. 6 (2003) B19–B22. doi:10.1149/1.1557033.

[77] X. Zhang, W. He, I. Odnevall Wallinder, J. Pan, C. Leygraf, Determination of instantaneous corrosion rates and runoff rates of copper from naturally patinated copper during continuous rain events, Corros. Sci. 44 (2002) 2131–2151. doi:10.1016/S0010-938X(02)00015-X.

[78] A. Srivastava, R. Balasubramaniam, Electrochemical impedance spectroscopy study of surface films formed on copper in aqueous environments, Mater. Corros. 56 (2005) 611–618. doi:10.1002/maco.200503866.

[79] Y.-C. Kuo, J.-W. Lee, C.-J. Wang, Y.-J. Chang, The effect of Cu content on themicrostructures, mechanical and antibacterial properties of Cr–Cu–N nanocomposite coatings deposited by pulsed DC reactive magnetron sputtering, Surf. Coatings Technol. 202 (2007) 854–860. doi:10.1016/J.SURFCOAT.2007.05.062.

[80] I. T. Hong, C. H. Koo, Antibacterial properties, corrosion resistance and mechanical properties of Cu-modified SUS 304 stainless steel, Mater. Sci. Eng. A. 393 (2005) 213–222. doi:10.1016/J.MSEA.2004.10.032.

[81] X.-Y. Zhang, X.-B. Huang, L. Jiangy, Y. Maa A.-l. FAN, B. Tang, Antibacterial Property of Cu Modified Stainless Steel by Plasma Surface Alloying, J Iron Steel Res Int, 19 (2012), 75-79. doi:10.1016/S1006-706X(12)60091-0.

[82] J. O. Noyce, H. Michels, C. W. Keevil, Potential use of copper surfaces to reduce survival of epidemic meticillin-resistant *Staphylococcus aureus* in the healthcare environment, J. Hosp. Infect. 63 (2006) 289–297. doi:10.1016/j.jhin.2005.12.008.